

PHYSICAL REVIEW LETTERS

VOLUME 45

8 DECEMBER 1980

NUMBER 23

Comparison of νn and νp Charged-Current Cross Sections from High-Energy Neutrino Interactions in Deuterium

J. Hanlon, R. A. Burnstein, and H. A. Rubin
Illinois Institute of Technology, Chicago, Illinois 60616

and

C. Y. Chang, T. Dombeck, G. A. Snow, D. Son, and P. H. Steinberg
University of Maryland, College Park, Maryland 20742

and

R. Engelmann, T. Kafka, and S. Sommars
State University of New York at Stony Brook, Stony Brook, New York 11794

and

T. Kitagaki, S. Tanaka, H. Yuta, K. Abe, K. Hasegawa, A. Yamaguchi, K. Tamai,
T. Hayashino, S. Kunori, Y. Ohtani, and H. Hayano
Tohoku University, Sendai 980, Japan

and

C. C. Chang, W. A. Mann, and J. Schneps
Tufts University, Medford, Massachusetts 02155
(Received 18 August 1980)

From an analysis of the reaction $\nu_\mu + d \rightarrow \mu^- + X$, obtained from an exposure of the Fermilab 15-ft deuterium-filled bubble chamber, the ratios of charged-current cross sections for $E_\nu > 10$ GeV are determined to be $\sigma(\nu n)/\sigma(\nu p) = 2.03 \pm 0.28$ for $\langle E_\nu \rangle = 50$ GeV, and $\sigma(\bar{\nu} n)/\sigma(\bar{\nu} p) = 0.51 \pm 0.16$ for $\langle E_{\bar{\nu}} \rangle = 40$ GeV. Bjorken- x distributions for neutron and proton targets show that the majority quark in the nucleon has a broader momentum distribution in the infinite momentum frame than does the minority quark.

PACS numbers: 13.15.+q

High-energy leptons have long been recognized as a powerful probe of the structure of nucleons,¹ as illustrated by the Stanford Linear Accelerator Center-Massachusetts Institute of Technology electroproduction experiments,² and by numerous high-energy neutrino experiments³ with nuclear or hydrogen targets. In this paper we present the first comparison of the deep-inelastic reactions $\nu_\mu + n \rightarrow \mu^- + X$ and $\nu_\mu + p \rightarrow \mu^- + X$ as deduced from the interactions of neutrinos with energy > 10 GeV

with deuterium targets. The ratio of cross sections for the corresponding $\bar{\nu}$ reactions are determined by using the small ($\sim 14\%$) $\bar{\nu}$ component of the beam.

Neutrino interactions were recorded in a 320 000-frame exposure of the Fermilab 15-ft bubble chamber filled with deuterium to a wide-band single-horn focused neutrino beam.⁴ In addition to the bubble chamber photographs, the recorded data include information from the ex-

ternal muon identifier⁵ (EMI). The analysis presented here is based on data from 105 000 frames, corresponding to a flux on target of 1.6×10^{18} protons of 350 GeV/c.

The film was scanned twice for interactions with ≥ 2 prongs produced by incident neutral particles of energy ≥ 2 GeV. All neutrino event candidates were measured and reconstructed with the geometry program TVGP. We accept for further analysis only those event candidates where the primary interaction occurs within a fiducial volume of 15.6 m³ and which have $\sum p_i > 5$ GeV/c, where p_i is the component of laboratory momentum in the beam direction and the sum is taken over all charged secondary particles. In addition, restrictions are imposed on two-prong event candidates to remove K^0 and Λ decays and γ conversions from the event sample. Appropriate multiplicity-dependent weights are applied to the data to account for scanning and processing losses; the average scanning times processing efficiency is 0.83.

Two independent sets of criteria were used to select samples of charged-current events. The first method uses a kinematic technique to identify negative muons from neutrino-induced events. The muon candidate is chosen to be that negative track in the event for which the quantity $F = p_i^- \vec{p}_{TR}^- \times [\sum (p_{TR}^i)^2]^{-1/2}$ is a maximum.⁶ In this expression p_i^- is the component of the μ^- candidate's momentum transverse to the incident neutrino direction, \vec{p}_{TR}^- is the component of its momentum transverse to the vector sum of the momenta of the other charged particles in the event, and $\sum (p_{TR}^i)^2$ is taken over all other charged particles in the event. We accept as neutrino charged-current events those in which the μ^- candidate has $p_{TR}^- > 1.0$ GeV/c.

The second method uses a two-plane EMI to identify both neutrino and antineutrino charged-current events. We accept as muons all tracks with momentum $p^\mu > 5.0$ GeV/c for which the χ^2 probability for the extrapolated trajectory to match time-coincident hits in both planes of the EMI is greater than 0.001. Each identified muon is weighted by the inverse of the acceptance of the EMI for tracks with the same charge, momentum, and polar angle as the muon. The average acceptance of the EMI for events with $p^\mu > 5.0$ GeV/c is 0.93.

The incident neutrino energy of the charged-current events identified by either event selection method is estimated by using transverse momentum balance⁷: $E_\nu = p_i^\mu + p_i^H + |\vec{p}_i^\mu + \vec{p}_i^H| p_i^H / p_i^\mu$,

where the symbols p^μ and p^H refer to the muon momentum and the vector sum of the charged hadron momenta, respectively. Only events with $E_\nu > 10$ GeV are accepted for analysis.

Two considerations are involved in determining the number of events in neutron-target and proton-target categories; one relating to the identification of events with a spectator proton and the other accounting for the effects of rescattering within the deuteron. We identify as spectator-proton (neutron-target) events those events with an invisible spectator proton (i.e., even-prong events) and those events with a stopping proton whose production angle θ_s is backward with respect to the beam direction in the laboratory. The unidentified forward-spectator-proton events are accounted for by weighting each observed backward-spectator-proton event by a factor $W_{\text{spect}} = 1 + \nu$. The quantity ν is the ratio of the product of the Möller flux factor and the neutrino cross section for an event with a forward spectator proton with production angle $\theta_s + \pi$ to the same product for the observed backward-spectator-proton event. The spectator-proton weights applied to the data are $W_{\text{spect}} = 1$ for invisible-spectator-proton events, $W_{\text{spect}} = 1 + [(E_s - p_s \cos \theta_s) / (E_s + p_s \cos \theta_s)]^2$ for backward-spectator-proton events, and $W_{\text{spect}} = 0$ for all others, where E_s and p_s are, respectively, the energy and momentum of the observed backward spectator proton. For the purpose of assigning the spectator-proton weights, stopping protons with momenta less than 200 MeV/c are treated as if they are invisible.

Separation of deuteron-target interactions into neutron-target and proton-target events is complicated by the phenomenon of rescattering, whereby the products of an interaction with one of the nucleons within the deuteron interact with the other nucleon. The correction for rescattering is important because it changes the topology of a neutron-target event to that of a proton-target event, while the topology of a rescattered proton-target event remains unchanged. We have estimated⁸ the fraction of neutrino-deuterium events which rescatter to be $f_{rs} = 0.094 \pm 0.035$ by extrapolating the rescatter rates observed in proton-deuterium and pion-deuterium interactions. Separate distributions for neutron-target and proton-target events are obtained by plotting each event first with a neutron-target weight $W_n = W_{\text{spect}} / (1 - f_{rs})$ and then with a proton-target weight $W_p = 1 - W_n$, compensating for the effects of both rescattering and spectator-proton identification. All data are corrected for small HD and H₂ con-

taminations in the bubble chamber liquid.

The final sample of kinematically selected neutrino charged-current events consists of 3857 events in which all charged tracks are successfully reconstructed by TVGP, while the EMI-selected samples consist of 1742 neutrino charged-current events and 105 antineutrino charged-current events. For the neutrino sample we find $\langle E_\nu \rangle = 50$ GeV, and for the antineutrino sample $\langle E_{\bar{\nu}} \rangle = 40$ GeV. On the basis of a 30 000-event Monte Carlo simulation, our observed distributions are corrected for a 21% event loss at $p_{\text{TR}}^- < 1.0$ GeV/c (kinematic selection) or 27% loss at $p^\mu < 5.0$ GeV/c (EMI selection). In addition, the kinematically selected ν sample is corrected for a 3.0% contamination due to neutral-current ν events and 1% due to $\bar{\nu}$ events.

The ratio of the νn to νp charged-current cross sections for $E_\nu \geq 10$ GeV is measured to be $R = \sigma(\nu n \rightarrow \mu^- X) / \sigma(\nu p \rightarrow \mu^- X) = 2.03 \pm 0.08 \pm 0.27$ using the kinematic selection technique, where the first error is statistical, and the second is systematic. This ratio, measured with the EMI selection method, is $R = 2.18 \pm 0.13 \pm 0.28$, in agreement with the result of the kinematic analysis. We prefer the kinematic method because of its lower statistical error. We observe no systematic variation of this ratio with ν energy in the range $10 \text{ GeV} < E_\nu < 200 \text{ GeV}$. The ratio of $\bar{\nu}$ charged-current cross sections measured with the EMI technique is $\bar{R} = \sigma(\bar{\nu} n \rightarrow \mu^+ X) / \sigma(\bar{\nu} p \rightarrow \mu^+ X) = 0.51 \pm 0.15 \pm 0.07$, in agreement with an earlier $\bar{\nu}$ -Ne measurement of 0.45 ± 0.08 .⁹ (The kinematic technique for selecting charged-current events fails because of the large ν background in the $\bar{\nu}$ sample.) The above ratios include correction factors arising from differing effects of the cuts on n - and p -target events, as determined from the Monte Carlo simulation, of 1.04 (kinematic selection), 1.06 (EMI ν event selection), and 0.89 (EMI $\bar{\nu}$ event selection).

The dominant uncertainty in this analysis is due to the uncertainty in the correction for rescattering. Before the correction for rescattering is applied, the spectator-proton-event to non-spectator-proton-event ratios are $R' = 1.54 \pm 0.05$ (kinematic ν selection), $R' = 1.64 \pm 0.08$ (EMI ν selection), and $\bar{R}' = 0.44 \pm 0.12$ (EMI $\bar{\nu}$ selection).

Our values of the charged-current cross-section ratios, $R = 2.03 \pm 0.08 \pm 0.27$ and $\bar{R} = 0.51 \pm 0.15 \pm 0.07$, are in agreement with the quark-parton-model (QPM) predictions of $R = 1.89$ and $\bar{R} = 0.58$ obtained by using the scaling quark structure functions deduced by Field and Feynman¹⁰ from

electroproduction data.

In the quark model the valence quarks are ddu in the neutron and uud in the proton. If we call d (u) the majority quark in the neutron (proton) and the minority quark in the proton (neutron), on the basis of charge symmetry we expect the majority (minority) quark distributions to be the same in the neutron and proton. The striking difference in the momentum fraction carried by the majority quark relative to the minority quark in the nucleon deduced from $e-p$ and $e-d$ experiments² is revealed here in the Bjorken- x distributions of charged-current νn events compared to νp events. Figure 1 displays the Bjorken- x distributions of the kinematically selected charged-current events for neutron and proton targets for $E_\nu > 10$ GeV and $W > 1.5$ GeV. The cut on W , imposed because the resolution in x is poor for events at low W , has the effect of removing elastic and quasielastic events from the sample. The observed distributions, before applying the Monte

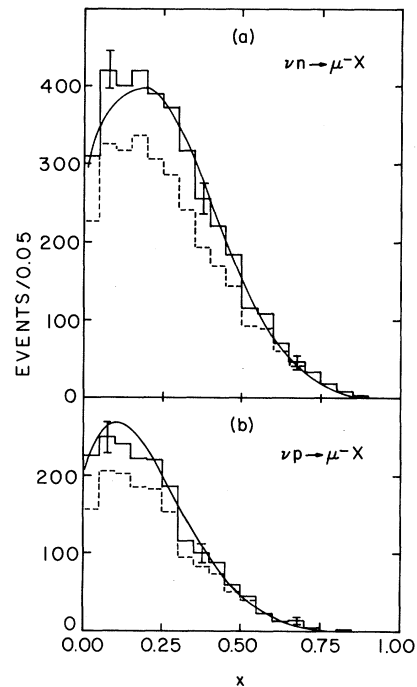


FIG. 1. Distributions of Bjorken- x for (a) the reaction $\nu_\mu + n \rightarrow \mu^- + X$ and (b) the reaction $\nu_\mu + p \rightarrow \mu^- + X$ for $E_\nu > 10$ GeV and $W > 1.5$ GeV. The broken-line histograms represent the observed distributions, while the solid-line histograms include Monte Carlo corrections for event losses and backgrounds resulting from the kinematic selection of charged-current events. The curves represent the QPM predictions with use of the scaling quark structure functions of Ref. 10.

Carlo corrections for event losses at $p_{TR} > 1 \text{ GeV}/c$ and the smearing of measured kinematic quantities due to the estimates of E_ν , are indicated by the broken-line histograms, while the solid-line histograms represent the corrected distributions. The curves, which represent the QPM predictions with use of the Field and Feynman scaling quark structure functions,¹⁰ are seen to agree well with the data.¹¹

In Fig. 2, νn and νp cross sections are compared with one another directly. Displayed in Fig. 2(a) are the Bjorken- x distributions for the two targets normalized to unit area. In the valence quark region ($x \gtrsim 0.25$), the d quark distribution in the neutron is seen to be broader than the d quark distribution in the proton. The difference between the shapes of those two distribu-

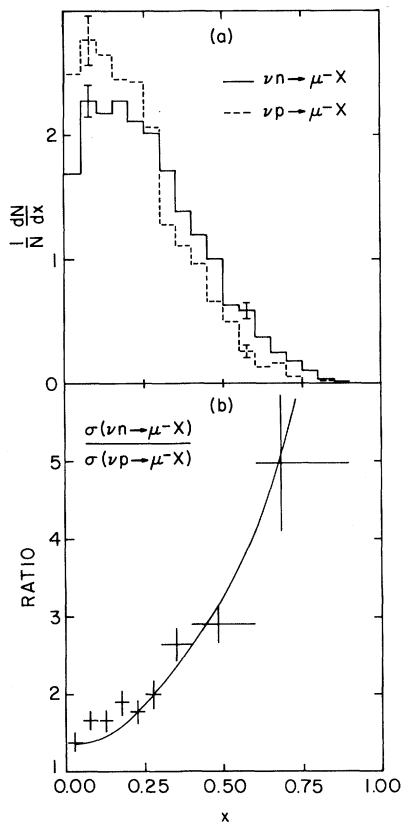


FIG. 2. Comparison of cross sections for the reactions $\nu_\mu + n \rightarrow \mu^- + X$ and $\nu_\mu + p \rightarrow \mu^- + X$ for $E_\nu > 10 \text{ GeV}$ and $W > 1.5 \text{ GeV}$. (a) Distributions of Bjorken- x normalized to unit area. (b) Ratio of the cross sections as a function of Bjorken x . The errors shown are statistical uncertainties only. The curve represents the QPM predictions with use of the scaling quark structure functions of Ref. 10.

tions is further illustrated in Fig. 2(b), where the ratio of νn to νp charged-current cross sections is displayed as a function of x . These observations, as well as those of the deep-inelastic ep - ed comparisons,² indicate that the majority quark in the nucleon has a broader momentum distribution in the infinite momentum frame than does the minority quark. This effect has been variously interpreted as an SU(6)-breaking effect related to the mass difference of the Δ and the nucleon,¹² and as a quantum chromodynamics gluon-exchange effect.¹³

Our results on charged-current interactions of ν and $\bar{\nu}$ with neutrons and protons can be summarized as follows: First, both the ratio of the total cross sections and the shapes of the x distributions are in agreement with the QPM predictions of Ref. 10. Second, the data on $d\sigma/dx$ reveal the quantitative difference between the majority and minority quark distributions in a clear and convincing manner.

We thank the members of the Accelerator Division and Neutrino Department at Fermilab for their assistance in conducting this experiment, with special appreciation to the 15-ft bubble chamber group, and to the Berkeley-Hawaii collaboration which constructed the EMI. We wish to thank the scanning and measuring personnel at each of our laboratories for their careful work. This research is supported in part by the U. S. National Science Foundation and the U. S. Department of Energy.

¹See, for example, R. P. Feynman, *Photon Hadron Interactions* (Benjamin, New York, 1972); C. H. Llewellyn Smith, *Phys. Rep.* **3C**, 261 (1972); G. Altarelli, *Nuovo Cimento* **4**, 335 (1974).

²See, for example, R. E. Taylor, in *Proceedings of the International Symposium on Lepton and Photon Interactions at High Energies, Stanford, California, 1975*, edited by W. T. Kirk (Stanford Linear Accelerator Center, Stanford, Cal., 1975), p. 343; A. Bodek *et al.*, *Phys. Rev. D* **20**, 1471 (1979), and references therein.

³See references listed by A. Para, in *Proceedings of the Ninth International Symposium on Lepton and Photon Interactions at High Energies, Batavia, Illinois, 1979*, edited by T. B. W. Kirk and H. D. I. Abarbanel (Fermilab, Batavia, Ill., 1979).

⁴S. Mori, Fermilab Reports No. TM-663, 1976 (unpublished), and No. TM-720, 1977 (unpublished); J. Grimson and S. Mori, Fermilab Report No. TM-824, 1978 (unpublished).

⁵R. J. Cence *et al.*, *Nucl. Instrum. Methods* **138**, 245 (1976).

⁶J. Bell *et al.*, Phys. Rev. D **19**, 1 (1979).

⁷H. G. Heilmann, University of Bonn, Internal Report No. WA21-int-1, 1978 (unpublished); J. Blietschau *et al.*, Phys. Lett. **87B**, 281 (1979).

⁸J. Hanlon *et al.*, in *Proceedings of Neutrino '79, International Conference on Neutrinos, Weak Interactions, and Cosmology, Bergen, Norway, 1979*, edited by A. Haatuft and C. Jarlskog (Fysik Institutt, Bergen, 1980), Vol. 2, p. 286.

⁹V. I. Efremenko *et al.*, Phys. Lett. **84B**, 511 (1979).

¹⁰R. Field and R. P. Feynman, Phys. Rev. D **15**, 2590 (1977).

¹¹If, instead of Bjorken x , the Nachtmann scaling variable $\xi = 2x/[1 + (1 + 4M^2x^2/Q^2)^{1/2}]$ is used, the distributions remain essentially the same.

¹²R. Carlitz, Phys. Lett. **58B**, 345 (1975).

¹³G. R. Farrar and D. R. Jackson, Phys. Rev. Lett. **35**, 1416 (1975).

Parity Nonconservation in Proton-Nucleus Scattering at 6 GeV/c

N. Lockyer, T. A. Romanowski, J. D. Bowman, C. M. Hoffman, R. E. Mischke,
D. E. Nagle, J. M. Potter, R. L. Talaga, E. C. Swallow,^(a)
D. M. Alde,^(b) D. R. Moffett, and J. Zyskind

Department of Physics, Ohio State University, Columbus, Ohio 43210, and University of California, Los Alamos Scientific Laboratory, Los Alamos, New Mexico 87545, and Department of Physics, Elmhurst College, Elmhurst, Illinois 60126, and Enrico Fermi Institute, University of Chicago, Chicago, Illinois 60637, and Department of Physics, University of Illinois, Urbana, Illinois 61801, and Argonne National Laboratory, Argonne, Illinois 60439, and W. K. Kellogg Radiation Laboratory, California Institute of Technology, Pasadena, California 91109

(Received 2 September 1980)

A parity-nonconservation asymmetry has been measured in the total cross section for 6-GeV/c polarized protons on a water target. The asymmetry $A_L = (\sigma_+ - \sigma_-)/(\sigma_+ + \sigma_-)$, defined as the fractional difference of total cross sections for positive- and negative-helicity protons on an unpolarized target, is $A_L = (2.65 \pm 0.60) \times 10^{-6}$. The quoted error includes both statistical and systematic contributions.

PACS numbers: 13.75.Cs, 11.30.Er

We have performed a search for parity nonconservation in proton-nucleus scattering at 6 GeV/c by studying the dependence of the total cross section on the helicity of the incident polarized proton beam. This dependence is expressed by the parity-nonconservation asymmetry $A_L = (\sigma_+ - \sigma_-)/(\sigma_+ + \sigma_-)$, where σ_+ (σ_-) is the total cross section for positive- (negative-) helicity protons on a water target. At present, investigation of parity-nonconserving phenomena is the only way to gain experimental knowledge of the strangeness-conserving hadronic weak interaction.

A parity-nonconservation asymmetry A_L can arise from the interference of the strong and weak interactions between nucleons. Measurements at low energies^{1,2} yield $A_L \approx 10^{-7}$ in agreement with calculations.³⁻⁵ The first measurement at 6 GeV/c found $A_L = (5 \pm 9) \times 10^{-6}$ with use of a beryllium target.⁶ A value of $A_L = (-15.0 \pm 2.8) \times 10^{-6}$ was obtained when the experiment was repeated with use of a water target.⁷ At that time, it was realized that a nonzero transmission asymmetry can result from the production and subsequent decay of longitudinally polarized hyperons. A focusing magnetic spectrometer was

added to eliminate hyperon-decay products.⁸ Here we report our most recent measurement $A_L = (2.65 \pm 0.60) \times 10^{-6}$ which is an order of magnitude larger than an existing prediction⁹ of $A_L \sim 10^{-7}$ for both pp and pn scattering.

This experiment used a vertically polarized proton beam from the Argonne National Laboratory zero-gradient synchrotron (ZGS). The beam had an average polarization $|\vec{P}| = 0.71 \pm 0.03$, an average intensity of 3.2×10^8 protons/pulse, a spill width of roughly 700 ms, and a repetition rate of 0.3 Hz. The polarization direction was reversed at the source between ZGS pulses. An upward bend of the beam rotated the polarization to a longitudinal direction. The horizontal position of the beam centroid at the target was stabilized with the aid of a feedback loop controlling the current in an upstream bending magnet.

A schematic representation of the experiment is shown in Fig. 1. The transmission Z through an 81-cm-long water target was measured by two independent detector systems which have been described previously.⁶ One system consisted of a pair of identical plastic scintillation counters, each viewed by four photomultiplier tubes. The